The Anharmonic Casimir Oscillator (ACO)—The Casimir Effect in a Model Microelectromechanical System

F. Michael Serry, Dirk Walliser, and G. Jordan Maclay, *Member, IEEE*

Abstract—**The sizes of and the separations between the components in some MEMS are already in the sub-micrometer regime [1], [2]. Further miniaturization is carrying the MEMS technology into a domain where some quantum mechanical effects, hitherto neglected, will need to be taken into account. When separations between objects are small enough, certain quantum effects become manifestly significant even if the masses of the objects are too large by quantum standards. The Casimir effect, for example, is the attractive pressure between two flat parallel plates of solids that arises from quantum fluctuations in the ground state of the electromagnetic field [3]–[5].[1] The magnitude of this pressure varies as the inverse fourth power of the separation between the plates.[2] At a 20 nm separation between two metallic plates, the attraction is approximately 0.08 atmosphere. If one or both plates are nonconducting, the pressure is smaller, roughly by an order of magnitude. As an idealized MEMS component that takes account of the Casimir effect, the Anharmonic Casimir Oscillator (ACO) is introduced and shown to be a bi-stable system for certain values of the dimensionless parameter, C, which characterizes the system. The phenomenon of "stiction" in MEMS is then explained as analogous to an ACO energetically descending to and settling in an equilibrium state that is very stable against perturbations for all values of C. A micromechanical switch based on the bistable ACO is proposed and modeled. The dynamics of an ACO, executing undamped periodic motion, are studied using numerical and analytical solutions of the differential equation of motion. Frequencies and amplitudes vary with C. C, in turn, is inversely proportional to the fifth power of the parallel plate separation. This extreme sensitivity makes the ACO an attractive platform for designing rather sensitive sensors and detector systems, such as submicrometer proximity sensors and microlever deflection detectors for scanning probe microscopes. [120]**

I. Introduction

IN IC fabrication, the minimum feature size has decreased by a factor of 2 every six years for nearly two decades (Fig. 1). The competition for delivering faster computing capability in smaller computers is pushing the research and development in lithography toward achieving yet smaller minimum feature sizes. No doubt, the much aspired to further miniaturization will carry over into the field of MEMS as well. Until now, the spacings between adjacent surfaces in MEMS have typically been of the order of a micrometer or larger. This picture has begun to change. As the dimensions between MEMS components decrease, there is a growing need for better understanding of interactions between micromachined surfaces at small separations. For example, the actuation scheme of choice in MEMS is often electrostatic. To generate larger actuating forces and torques with smaller applied voltages, submicrometer separations are desirable [1]. On the other hand, even at separations of the order of a micrometer there has been repeated occurrence of the unwanted "stiction" phenomenon, wherein a thin micromachined membrane or cantilever has been observed to unexpectedly latch onto an adjacent parallel surface and remain attached to that surface [11], [12]. The proliferation of smaller and lighter components and the reduction of the separations between these components will require MEMS designs to account for some effects that have been neglected until now.

One such effect, arising in devices that are subjected to capillary forces during wet etching of sacrificial layers, was discussed recently in this JOURNAL [13]. A less familiar one is the parallel plate Casimir effect. With the Casimir effect

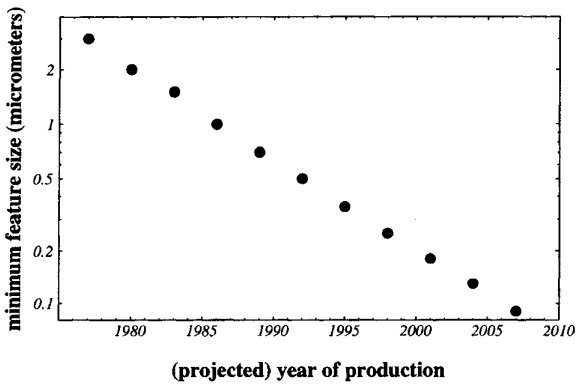

Fig. 1. Reduction of IC feature size. The minimum feature size on IC's has been reduced by a factor of 2 approximately every six years. (Source: Chenming Hu, "Mosfet scaling in the next decade and beyond," *Semiconductor International*, vol. 17, no. 6, pp. 105–114, June 1994.)

Manuscript received July 11, 1994; revised May 12, 1995. Subject Editor, R. O. Warrington.

F. M. Serry and G. J. Maclay are with The Microfabrication Applications Laboratory, Department of Electrical Engineering & Computer Science, The University of Illinois at Chicago, Chicago, IL 60607 USA

D. Walliser is with the Microfabrication Division, Daimler Benz Company, Frankfurt, Germany.

IEEE Log Number 9415187.

[1]There exists a larger class of Casimir forces, of which the parallel plate Casimir force is an example. These forces are all quantum mechanical in origin. Casimir forces may be attractive or repulsive, depending on the geometry of the surfaces [6], [7].

[2]The parallel plate Casimir pressure is identical to the retarded van der Waals attractive pressure between two parallel plates [8]–[10].

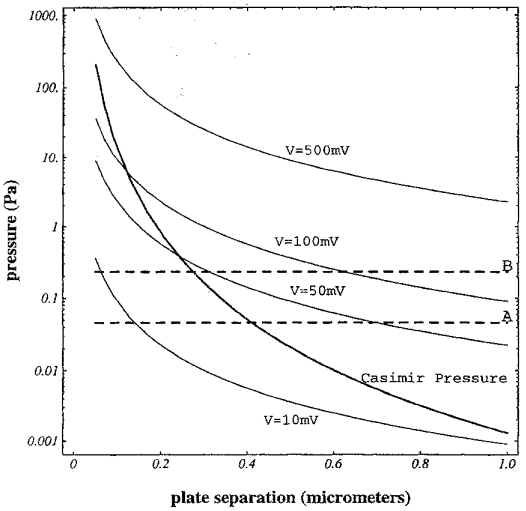

Fig. 2. Casmir, electrostatic, and gravitation pressures. A comparison of the attractive pressures due to the Casimir effect and applied electrostatic voltage (V) between two flat parallel plates of conductors in vacuum. Also shown are the gravitational pressure on 2-μm-thick (dashed line A) and 10-μm-thick (dashed line B) silicon membranes.

in focus, in this paper we show that such effects may be amenable to functionality when they are well understood and exploited. The Casimir effect is the attraction between two infinitely extended, parallel, flat plates that comes about due to the quantum fluctuations in the zero point electromagnetic field [1]–[3].[3] In the presence of the plates, the boundary conditions on the electromagnetic field are altered from the free field conditions. As a consequence, the vacuum electromagnetic energy density in the space between the opposing parallel plates is less than that outside of this space. The resulting energy density difference gives rise to the attractive Casimir pressure between the plates. The fundamental notion of a force due to quantum fluctuations is quite general and applies to other geometries. The force between the interacting bodies is sometimes repulsive, depending on the geometry of the system [6], [7]. This class of forces is collectively referred to as the Casimir forces. There is an extensive body of published literature on theoretical and experimental work on the Casimir effect, as well as a renewed interest in the whole class of interactions due to quantum fluctuations [3]–[10], [14]–[27].

In the simple parallel plate geometry, the Casimir pressure is the same as the retarded van der Waals pressure [10]. For very small separations (typically below 20 nm), the retardation, which is a result of the finite propagation speed of the electromagnetic field, is not significant; in this case the ordinary nonretarded van der Waals pressure, which varies as

[3]If the separation between the plates is much smaller than the lateral dimensions of the plates (we estimate at least two orders of magnitude smaller) the infinite extension of the plates is well approximated. Small departures from the parallel geometry and from flatness are apparently allowed as demonstrated experimentally [17]–[19]. The exact degree of sensitivity of the parallel plate Casimir effect to these departures has been studied theoretically by some groups [14]–[16]. We have found no published results of experimental investigations on this subject.

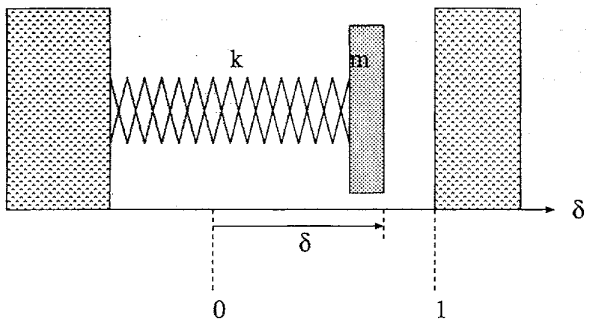

Fig. 3. The Anharmonic Casimir oscillator. Due to the Casimir effect, the moveable flat plate on the left, at $\delta < 1$, is attracted to the stationary flat surface parallel to it on the right. The wall on the left is far from the movable plate and the linear restoring force due to the spring is zero at $\delta = 0$.

the inverse cube of the separation, is present [8]–[10], [18]. When the free space plate separation, "d," is large enough (i.e., 20 nm or larger) so that the retardation is pronounced, and at low temperatures ($d \ll \hbar c/kT$, where c is the speed of light in vacuum, $\hbar$ is Planck's constant divided by 2π, k is Boltzmann's constant, and T is the absolute temperature), the attractive Casimir pressure, P_C, is given by

$$P_C = \eta \frac{\Re}{d^4} \tag{1a}$$

and

$$0 < \eta \leq 1 \tag{1b}$$

where the parameter η depends on the static electric permittivity of the plates and the constant of proportionality, $\Re$, is defined as

$$\Re \equiv \frac{\hbar c \pi^2}{240}. \tag{1c}$$

When both plates are perfectly conducting, η equals unity [8], [9]. Then, the pressure, P_C, is equal to $0.0013/d^4$ Pa (N/m^2) when the separation, d, is given in micrometers. This pressure is 208 Pa when d is 50 nm. For two plates made of silicon, the approximate value of η can be calculated to be 0.38 [8], [9]. This value can also be extracted from the experimental results in [18]. Fig. 2 shows the variation with plate separation of the Casimir pressure and of an attractive electrostatic pressure due to an applied dc voltage "V" across a parallel plate capacitor in vacuum for four different values of V. For reference, the gravitational pressure on a 2 μm and a 10-μm-thick single crystal silicon membrane (volume mass density = 2330 kg/m^3) are also shown, in dotted lines.

Although (1a) has been derived assuming perfectly parallel plates, experimental evidence suggests that some departure from the parallel geometry is permissible [17]–[19]. In fact, to date almost all experiments that have measured the Casimir pressure in agreement with (1a) have substituted at least one curved surface (e.g., a convex lens) for a flat plate. The limits of departure from the parallel geometry at which (1a) no longer holds have been the subject of some theoretical studies [14]–[16].

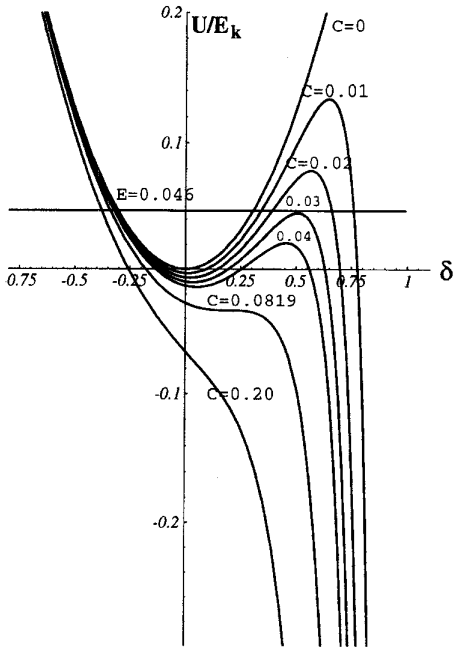

Fig. 4. The normalized potential energy per unit area of the parallel plates. $C = 0$ corresponds to the absence of the Casimir effect; this reduces the system to a simple harmonic oscillator. For $C < C_{\rm cr}(= 0.0819)$, the potential energy curve displays a pair of local extrema, corresponding to a stable and an unstable equilibrium state of the system. At $C = C_{\rm cr}$, there is an inflection point at $\delta = 0.2$. Finally, for $C > C_{\rm cr}$ no local extrema exist.

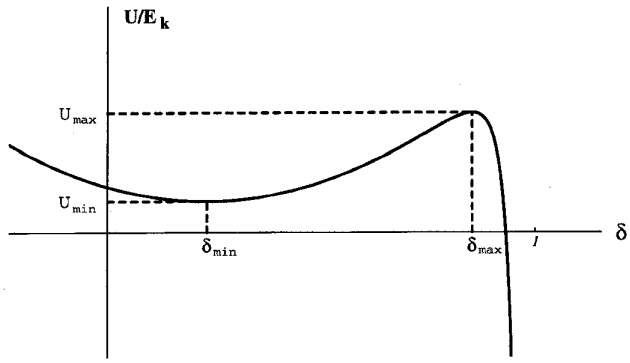

Fig. 5. For a given $C < C_{\rm cr}$ (e.g., $C = 0.04$), the normalized potential energy has a local maximum, $U_{\rm max}$, at $\delta_{\rm max}$, and a local minimum, $U_{\rm min}$, at $\delta_{\rm min}$. For perfectly smooth surfaces, the absolute minimum of the potential energy is infinitely large and negative and is located at $\delta = 1$.

In this paper, we will argue that the Casimir effect may be in part responsible for stiction in MEMS. Furthermore, we will show that even in systems that do not exhibit stiction, the Casimir effect may play an important role if the separations are small enough. We assume that (1a) is valid for geometries where the lengths and the widths of the parallel plates are finite but much greater than the separation, d, between them. The modeling is applicable to separations greater than or equal to about 20 nm. We present an analytical-computational model of the "ACO," which we believe to be the first dynamic system that takes into account the Casimir effect. We assume that we can describe the system dynamics using classical mechanics since the masses of the typical MEMS components are comparatively large. For simplicity, we will model our system with η set to unity. The results may be applied to nonconducting plate configurations by simply inserting the appropriate value of the parameter η where needed. This parameter can be calculated for a given system using formulae and graphs in [8] or [9]. For a handful of MEMS materials, experimental values for η can be extracted from the data in [18].

II. General Characteristics of the ACO

The geometry of the ACO is depicted in Fig. 3, where the parallel plate configuration is defined by the stationary plate on the right with a flat surface at $\delta = 1$ and the moveable plate on the left with its flat surface at $\delta < 1$. In this figure, $\delta = 0$ denotes the normalized equilibrium position of the movable plate in the absence of the Casimir pressure (i.e., in the absence of the stationary plate on the right) and corresponds to the unstretched state of the spring. The moveable plate has but one degree of freedom; it can only translate along the δ axis. The normalized displacement, δ, of the moveable plate is defined as the ratio of the nonnormalized displacement, w, of the moveable plate to the nonnormalized position, $w_0(> 0)$, of the stationary plate

$$\delta \equiv \frac{w}{w_0}. \tag{3}$$

The restoring pressure due to the spring of elasticity constant "k" (dimensions force per unit length per unit area) is linear in the displacement δ.

In the presence of the Casimir effect, the pressure $P(\delta)$ on the moveable plate arises from two contributions: P_k due to the elastic spring and P_C due to the Casimir effect[4]

$$P(\delta) = P_k(\delta) + P_C(\delta) = -kw_0\delta + \frac{\Re}{w_0^4(1-\delta)^4}. \tag{4}$$

We assume the system is conservative and define the potential energy, $U(\delta)$, per unit area of the moveable plate surface facing the stationary plate such that $P(\delta) \equiv -\frac{1}{w_0}\frac{\partial U(\delta)}{\partial \delta}$. Then $U(\delta)$ is found to be

$$U(\delta) = U_k(\delta) + U_C(\delta) = E_k\left(\frac{1}{2}\delta^2 - \frac{1}{3}\frac{C}{(1-\delta)^3}\right) \tag{5}$$

where U_k and U_C correspond to P_k and P_C, respectively. The unit of elastic energy, E_k, and the positive dimensionless characteristic constant, C, are defined below

$$E_k \equiv kw_0^2 \tag{6a}$$

$$C \equiv \frac{\Re}{kw_0^5}. \tag{6b}$$

[4]At separations below 20 nm between plates with atomically smooth surfaces, the attractive interaction between the plates is not well described by (1a) and therefore (4) is not valid. For these cases, the system's behavior is not well quantified by the rest of the mathematical analysis in this paper. The same may be said about the cases wherein the roughness of the surfaces is comparable to the mean separation; then, the attractive force may be a complex function of the surface topology and (1a) and (4) are again invalid.

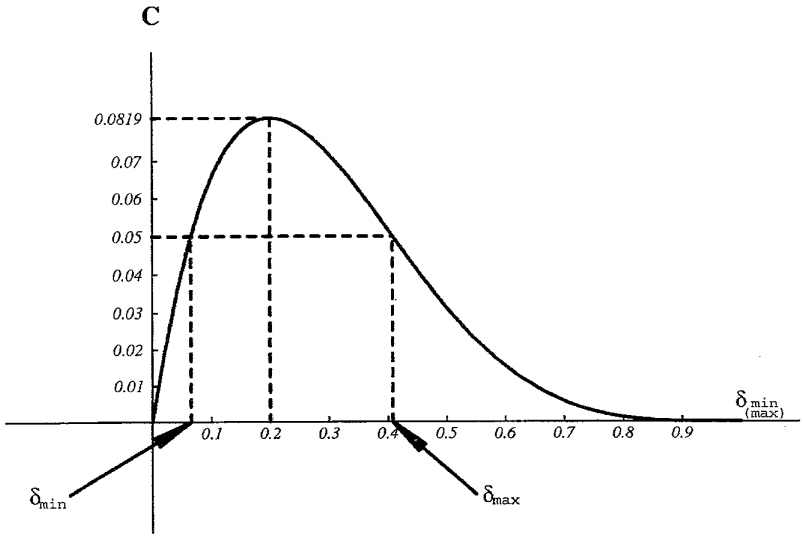

Fig. 6. For $C < C_{cr}$, the minimum of the potential energy is always located at $\delta_{min} < 0.2$, and the maximum at $\delta_{max} > 0.2$.

The relevant physical interpretation of C is the ratio of the force on the movable plate due to the Casimir Effect at no deflection (i.e., at $w = 0$) to the force on the movable plate due to the stretched spring at full deflection to the right (i.e., $w = w_0$). Fig. 4 shows several normalized potential energy curves for different values of the parameter C. The horizontal line denoted by "$E = 0.046$" represents an arbitrarily chosen energy level for the ACO. This line will be used in Section III.

For C greater than the critical value $C_{cr}(= 0.0819)$, the moveable plate collapses into the stationary plate, located at $\delta = 1$, regardless of the initial separation between the two. Fig. 5 shows that for $0 < C < C_{cr}$, the normalized potential energy has a local minimum, $U_{min}\,(\equiv U(\delta_{min})/E_k)$, at δ_{min}, which is closer to the origin of the δ-axis than to the stationary plate, and a local maximum, $U_{max}\,(\equiv U(\delta_{max})/E_k)$, at δ_{max}, closer to the edge of the stationary plate at $\delta = 1$. These extremes correspond to a stable and an unstable equilibrium state of the system, respectively

$$\left.\frac{\partial U(\delta)}{\partial \delta}\right|_{\delta_{\substack{\min\\(\max)}}} = 0, \tag{7a}$$

$$0 < C < C_{cr}. \tag{7b}$$

We define a "separation state" of the ACO as one in which the moveable plate is located at or oscillating about the stable equilibrium state at δ_{min} and does not have sufficient kinetic energy to move to the right, past δ_{max}.

With C subject to condition (7b), we insert $U(\delta)$ from (5) into (7a) to obtain an expression that relates a given value of C to a corresponding pair of δ_{min} and δ_{max} values

$$\delta_{\substack{\min\\(\max)}}\left(1 - \delta_{\substack{\min\\(\max)}}\right)^4 = C. \tag{8}$$

Fig. 6 is a graph corresponding to (8). As C approaches $C_{cr}(= 0.0819)$ from below, the shape of the potential energy curve changes (Fig. 4) such that the local extrema, located at δ_{min} and δ_{max}, converge to and are finally replaced by the inflection point at $\delta = \delta_{min} = \delta_{max} = 0.2$, which occurs when $C = C_{cr}$. For C greater than C_{cr}, there are no local extrema. Fig. 6 also shows that for all values of $0 < C < C_{cr}$, such as 0.05, the corresponding values for δ_{min} and δ_{max} are smaller and larger than 0.2, respectively.

The potential energy also has an absolute minimum at $\delta = 1$ for all values of C, as depicted in Fig. 4. If the parallel plates had perfectly smooth surfaces, this minimum would be infinitely deep. In a real device, however, which may be approximately modeled as an ACO with less than perfectly smooth surfaces, the effective depth of this minimum is finite because the asperities on the opposing parallel surfaces will always ensure a nonzero normalized minimum gap, ξ, between the plates; we shall refer to such a system as an "ACO device" hereafter.[5] Now we define the "contact state" of an ACO device as that state in which the moveable plate has collapsed into the stationary plate so that $\delta = 1 - \xi$. An ACO device in its contact state is a simple, yet plausible, picture that can explain, for example, the unfortunate fate of a thin silicon (or other) membrane or cantilever beam that is designed to function as a transducer but is pushed too close to an adjacent flat surface by a larger-than-expected signal. Capillary forces encountered during the wet fabrication of some MEMS have been shown to draw parallel surfaces into an unexpected intimate contact [11], [12], which remains even after the liquids evaporate. This sustained contact may also be explained as the consequence

[5]For an ACO device, the meaning of δ is modified as follows. We imagine an infinitely smooth flat plane inside the moveable plate and perpendicular to the δ axis. δ now stands for the position of this imaginary plane along the δ axis. Also, $\delta = 1$ is now the position of a similar plane inside the stationary plate. It is the distance between these two imaginary planes that now defines the parallel plate separation, which is finite, but approaches zero as the normalized mean surface roughness, $\xi/2$, on the two plates decreases. At contact, the expression for the attraction between the plates may be a complex one, depending on the topology of the rough surfaces. Even prior to contact (at separations below about 20 nm for atomically smooth surfaces), the attractive pressure may vary with the inverse third, rather than fourth, power of the separation. The practical limit of applicability of (1a) near contact depends on the surface roughness, and for atomically smooth surfaces such as mica the model has to take into account the transition from the retarded to the nonretarded regime.

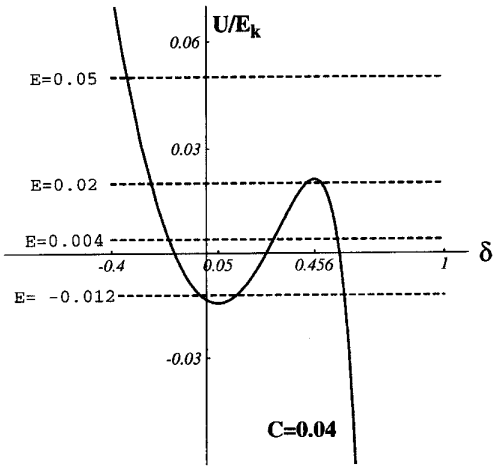

(a)

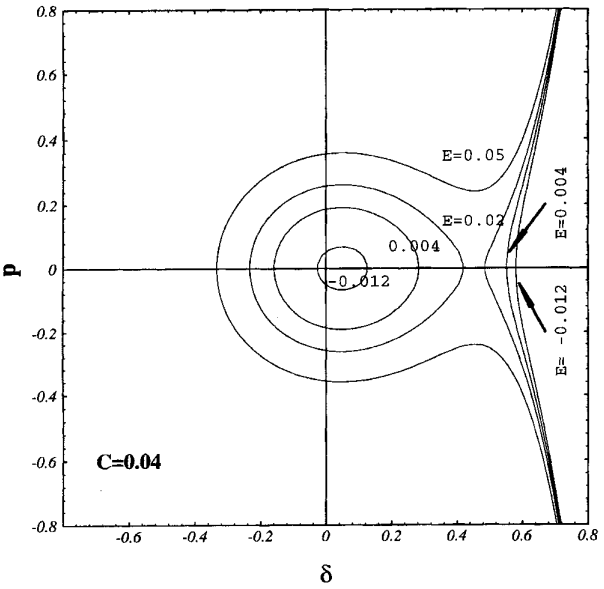

(b)

Fig. 7. (a) With C fixed ($= 0.04$) and for $U_{\min} < E < U_{\max}$, the local maximum of the potential serves as a classical barrier that confines the ordinate of the moveable plate either to the left or to the right of $\delta_{\max}$. (b) Phase space orbits corresponding to the energy levels depicted in (a). For $U_{\min} < E < U_{\max}$, there is a separation branch and a contact branch for each energy level. In the absence of the Casimir effect, the smallest separation orbit shown would be a perfect circle, centered at the origin of the coordinate system, while the corresponding contact branch would be missing.

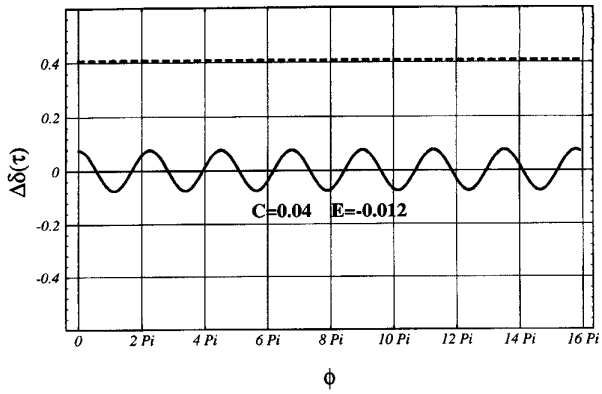

(a)

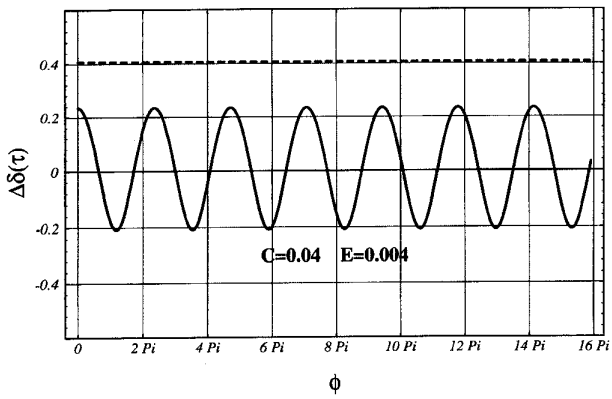

(b)

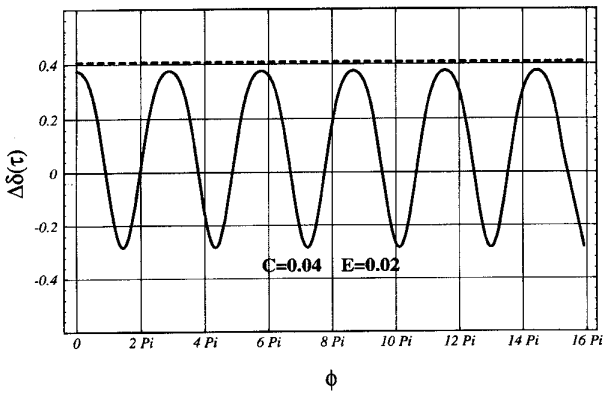

(c)

Fig. 8. Numerical solutions, in the normalized-time domain, of the differential equation (9) for $C = 0.04$ at the three lowest energy levels shown in Fig. 7(a). Departure from harmonicity is noticeable for $E = 0.02$.

of the parallel plate system "falling" into and subsequently remaining in the attractive potential well, due in part to the presence of the Casimir effect, where the elasticity forces are insufficient to restore separation.

For $C < C_{\rm cr}$, the equilibrium state at $\delta_{\min}$, along with the contact state at $\delta = 1 - \xi$, render an ACO device a bi-stable system that may, after some modifications, define a functional switch—the Casimir switch. Before presenting the Casimir switch in Section IV, we study some of the dynamic properties of the ACO.

III. Dynamics of the ACO

A. Energy Considerations

The differential equation of motion for an ACO in the absence of dissipative forces is

$$m\, w_0 \frac{\partial^2 \delta(t)}{\partial t^2} + \frac{1}{w_0} \frac{\partial U(\delta)}{\partial \delta} = 0 \qquad (9)$$

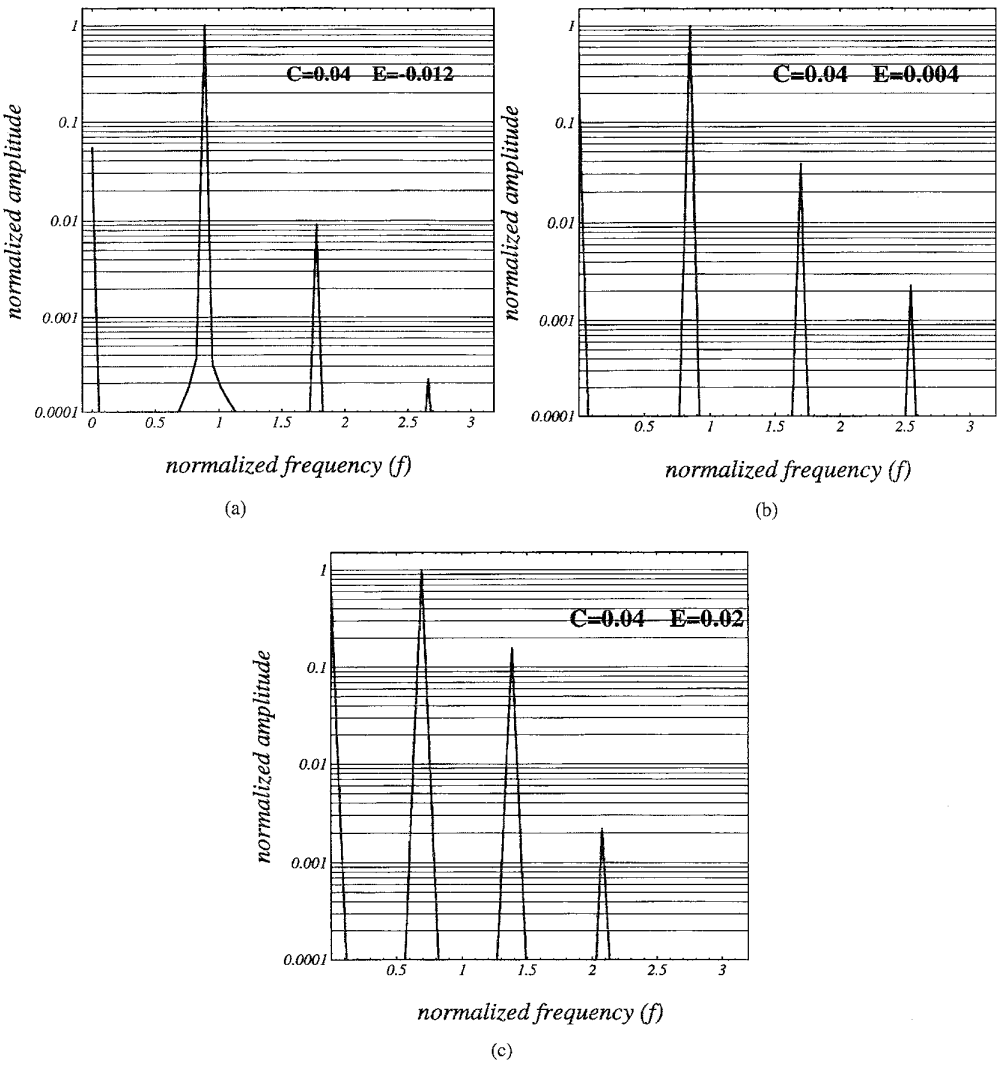

Fig. 9. Discrete Fourier spectra of the time domain oscillations in Fig. 8. All the amplitudes in a given spectrum are normalized to that of the fundamental frequency in that spectrum.

where m is the mass of the movable plate per unit area of that surface that faces the stationary plate (Fig. 3), and t denotes the time. Equation (9) is multiplied by $w_0 \frac{\partial \delta}{\partial \tau} d\tau$ and integrated once with respect to the re-scaled time $\tau (\equiv \sqrt{1/mt})$ to obtain the equation for the conservation of the total mechanical energy, E, which is normalized by the elastic energy E_k in (10)

$$\frac{1}{E_k}\left[\frac{w_0^2}{2}\left(\frac{\partial \delta(\tau)}{\partial \tau}\right)^2 + U(\delta)\right] = \text{constant} \equiv E. \qquad (10)$$

For a given value of $C < C_{\text{cr}}$, Fig. 7(a) indicates that the motion can exhibit different characteristics for different values of the normalized energy E. In this figure, where the potential energy curve is for $C = 0.04$, we see that for $U_{\min} < E < U_{\max}$, the local maximum of the potential serves as a classical barrier that confines the position, δ, of the moveable plate either to the left or to the right of $\delta_{\max}$. For $\delta > \delta_{\max}$, the moveable plate is expected to be bound closely to the stationary plate at $\delta = 1$. For $\delta < \delta_{\max}$, as long as E remains well below $U_{\max}$, we expect nearly harmonic motion with the classical turning points, δ_t, given by $U(\delta_t)/E_k = E$. When E is marginally less than $U_{\max}$, e.g., $E = 0.02$ in Fig. 7(a), we expect the motion to exhibit marked departure from harmonicity for $\delta < \delta_{\max}$. When $E > U_{\max}$, the barrier will not confine the motion of the movable plate.

A study of the phase space orbits corresponding to the energy levels in Fig. 7(a) help in clarifying the nature of the motion. This can be seen in Fig. 7(b), wherein the quantities plotted on the axes are the normalized position, δ, and the normalized momentum p, which is defined as $p \equiv \frac{1}{\sqrt{k}} \frac{\partial \delta}{\partial \tau}$, of the moveable plate. For three of the arbitrarily selected energy levels in Fig. 7(a), i.e., for $E = -0.012, 0.004$, and 0.02, the corresponding left branch orbits in Fig. 7(b) are closed and represent bound, periodic motion. We shall refer

to these closed branches as "separation branches" in reference to the separation of the parallel plates during the motion of the movable plate. Each of these three energy levels also has a right branch orbit, representing motion closer to (or in contact with) the stationary plate; these branches will be called "contact branches" since the movable plate contacts the stationary plate $\delta = 1$ [not shown in Fig. 7(b)]. The separation branch orbit of the lowest energy state shown, $(E = -0.012)$, indicates nearly simple harmonic motion. In the absence of the Casimir effect, this branch will be a perfect circle, centered at the origin of the coordinate system where $\delta = p = 0$, while the corresponding contact branch orbit would be absent. For the next energy state depicted $(E = 0.004)$, the separation branch orbit exhibits more asymmetry, indicating stronger anharmonicity. At $E = 0.02$, the separation branch is significantly elongated and is close to merging with the corresponding contact branch orbit on the right. For $E = 0.05\,(>U_{\max})$, the left and right branch orbits have merged; the corresponding motion would be that of the moveable plate falling, regardless of its initial position, into the deep attractive Casimir potential well and colliding with the stationary plate. In an ACO device, when the moveable plate with its finite kinetic energy $(p > 0)$ hits the stationary plate, it would probably be reflected with some loss of energy and reappear on a lower energy orbit at the bottom of the phase space plot $(p < 0)$. After several reflections, the kinetic energy would dissipate completely and the moveable plate would sustain contact with the stationary plate.

We can also envision the situation in which E is kept constant, while the value of C is altered, as depicted in Fig. 4. For example, assume $E = 0.046$ and $C = 0.02$, and that the moveable plate is in the separation state. If C were now increased to 0.03 or a larger value, with no change in the energy E, the height of the potential energy barrier would decrease such that at the new $\delta_{\max}$ the movable plate would have enough kinetic energy to continue on to the right, past the lowered potential energy barrier, and collide with the stationary plate. This feature can be exploited as a switching mechanism in a micromechanical switch (see Section IV).

B. Anharmonic Oscillations in Separation States

We now consider the oscillations of an ACO in separation states. We defined

$$\delta(\tau) \equiv \delta_{\min} + \Delta\delta(\tau)$$

with $\Delta\delta(\tau)$ denoting the normalized deflection of the moveable plate from $\delta_{\min}$, which is related to C through (8).

For $C = 0.04$, the numerical solutions of the differential equation of motion (9) for $\Delta\delta(\tau)$ and the corresponding discrete Fourier spectra.[6] are plotted in Figs. 8 and 9 for three of the energy values in Fig. 7. The horizontal axes in Fig. 8 correspond to the quantity $\sqrt{k}\tau(=\sqrt{\frac{k}{m}}t)$, which we define as ϕ. The value of $\Delta\delta(\tau)$ at the dashed lines in Fig. 8 equals $\delta_{\max} - \delta_{\min}$. These solutions are exact to within the limitations of the computational techniques employed [28]. For $E = -0.012$, Fig. 8(a) shows the motion as very nearly simple harmonic; the normalized period of oscillation for this plot is $\mathbf{T} \cong 1.1$.[7] The peak amplitude in the corresponding Fourier spectrum [Fig. 9(a)] appears at the normalized fundamental frequency, $\mathbf{f}_0 \cong 0.9$ ($\mathbf{T} = 1, \mathbf{f}_0 = 1$ for a simple harmonic oscillator). The spectrum also shows peaks at zero, $2\mathbf{f}_0$, and $3\mathbf{f}_0$. Fig. 9(b) shows that the relative contributions of the zero frequency term and the harmonics of the fundamental frequency increase as E increases to 0.004. In Fig. 8(c) $(E = 0.02)$, the motion shows noticeable departure from simple harmonicity with a rounding of the plot for large positive values of $\Delta\delta(\tau)$ where the moveable plate is close to $\delta_{\max}$. The increased period reflects the stronger influence of the Casimir effect. Also, the spectrum [Fig. 9(c)] shows a significant reduction in the value of the fundamental frequency, as well as sizable contributions at zero frequency and at $2\mathbf{f}_0$ and $3\mathbf{f}_0$. These features are consistent with the shape of the separation branch orbit corresponding to $E = 0.02$ in the phase space [Fig. 7(b)]. With E approaching $U_{\max}$, the growth of the zero frequency term can be viewed as corresponding to an increase in the mean amplitude that arises because the moveable plate spends more time at larger positive values of δ, near $\delta_{\max}$.

Next, in order to explore the dynamics of the ACO in separation states more fully, the method of successive approximations is used to find an approximate analytical solution to the differential equation of motion. We use a four term Taylor series expansion of the first derivative of the potential energy

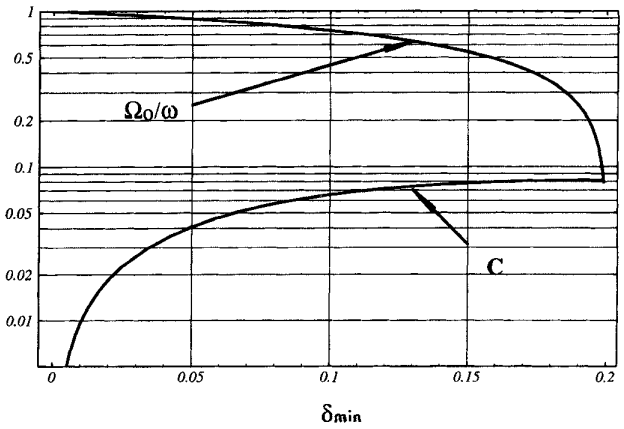

Fig. 10. Variation of C and Ω_0, the frequency of oscillation in the quadratic approximation of the potential, with $\delta_{\min}$. $\omega(=\sqrt{k/m})$ is the natural frequency of the harmonic oscillator in the absence of the Casimir effect.

[6]The discrete Fourier transform, "b_s," of a list of data points "a_r" of length "n" in a $\Delta\delta(\tau)$ versus $\phi(\equiv\sqrt{k}\tau)$ graph (Fig. 8) is defined as $\frac{1}{\sqrt{n}}\sum_{r=1}^{n} a_r\, e^{2\pi i(r-1)(s-1)/n}$ and is plotted, after the necessary rescaling and shifting of the frequency axis, in an amplitude versus normalized frequency ($\mathbf{f}$) graph (Fig. 9) [28]. All amplitudes in each spectrum are normalized to that of the fundamental frequency mode in that spectrum.

[7]The normalized period $\mathbf{T}$, and the normalized frequency, $\mathbf{f}$, are related to the nonnormalized period, T, and the nonnormalized frequency, f, as $\mathbf{T} = 2\pi\sqrt{\frac{m}{k}}\mathbf{T}$, $f = \frac{1}{2\pi}\sqrt{\frac{k}{m}}\mathbf{f}$.

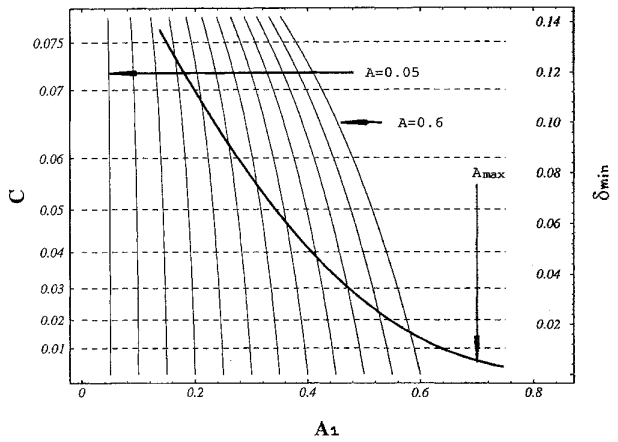

Fig. 11. Contour plots for the sum of the amplitudes $A(= A_0 + A_1 + A_2 + A_3)$. For a given value of C (or $\delta_{\min}$), the maximum allowed value for A in separation state oscillations is given by the three-way intersection of the $A_{\max}$ curve, the dashed line corresponding to the C value of interest, and one of the contour lines. The contour lines depicted represent the A values 0.05, 0.1, 0.15, 0.2, 0.25, 0.30, 0.35, 0.40, 0.45, 0.50, 0.55, and 0.60. For example, for $C = 0.04$, the maximum allowed value of A is 0.45. The contribution of A_1 to this value of A can be read from the horizontal axis. This is approximately 0.41. This value of A_1 can then be used in Fig. 12 to find the corresponding values for the three-term approximation of the frequency, Ω, as well as the amplitudes A_0, A_2, and A_3.

[see (5)] about $\delta_{\min}$

$$\frac{1}{w_0}\frac{\partial U(\delta)}{\partial \delta} \cong \frac{1}{w_0}\left[U'|_{\delta_{\min}} + U''|_{\delta_{\min}}\Delta\delta(t) + \frac{1}{2}U'''|_{\delta_{\min}}(\Delta\delta(t))^2 + \frac{1}{6}U^{(4)}|_{\delta_{\min}}(\Delta\delta(t))^3\right] \quad (11)$$

where $\delta(t) = \delta_{\min} + \Delta\delta(t)$, and a prime denotes the partial derivative with respect to δ. The first term in the series expansion vanishes, and we define the remaining expansion coefficients as follows:

$$\chi \equiv U''|_{\delta_{\min}} \quad (12a)$$

$$\alpha \equiv \frac{1}{2}U'''|_{\delta_{\min}} \quad (12b)$$

$$\beta \equiv \frac{1}{6}U^{(4)}|_{\delta_{\min}}. \quad (12c)$$

Substituting this expansion in (9), we look for a series solution for the differential equation. We write the solution in the form

$$\Delta\delta(t) = \Delta\delta_1(t) + \Delta\delta_2(t) + \Delta\delta_3(t) + \cdots \quad (13)$$

and start with the time harmonic Ansatz

$$\Delta\delta_1(t) = A_1\cos(\Omega t) \quad (14a)$$

where $\Omega(=2\pi f)$ is the exact nonnormalized angular frequency of oscillation of the ACO which in turn is written as a series sum

$$\Omega = \Omega_0 + \Omega_1 + \Omega_2 + \cdots. \quad (14b)$$

Ω is equal to Ω_0 if we use the linear approximation of the series expansion in Eq. 11 [29]. This would correspond to a quadratic approximation for the potential. The expression for Ω_0 is then given as

$$\Omega_0\frac{1}{w_0}\sqrt{\frac{\chi}{m}}\left(=\sqrt{\frac{k}{m}}\left[1 - \frac{4\delta_{\min}}{1-\delta_{\min}}\right]^{1/2}\right) \quad (15)$$

where the expression inside the parentheses is obtained by applying the definition (12a) to (5) and then substituting for C from (8). The successive terms in the series in (13) and (14b) are calculated using a variation of the method of successive approximations that requires the vanishing of the amplitudes of the resonant term contributions to the series solution in (13) [29]. The first correction to Ω_0 vanishes, and the second correction is found to be quadratic in A_1

$$\Omega_1 = 0, \quad (16a)$$

$$\Omega_2 = \Omega_0\left[\frac{3}{8}\frac{\beta}{\chi} - \frac{5}{12}\left(\frac{\alpha}{\chi}\right)^2\right]A_1^2. \quad (16b)$$

The first two corrections to the time harmonic Ansatz are found to be

$$\Delta\delta_2(t) = A_0 + A_2\cos(2\Omega t) \quad (17a)$$

and

$$\Delta\delta_3(t) = A_3\cos(3\Omega t) \quad (17b)$$

where the zero frequency or constant displacement term, A_0, and the amplitudes of the higher harmonics vary as the second and the third powers of A_1[8]

$$A_0 \equiv -\frac{\alpha}{2\chi}A_1^2 \quad (18a)$$

$$A_2 \equiv \frac{\alpha}{6\chi}A_1^2 \quad (18b)$$

$$A_3 \equiv \left[\frac{\alpha^2}{48\chi^2} + \frac{\beta}{32\chi}\right]A_1^3. \quad (18c)$$

The dependence of the exact fundamental frequency, Ω, on the amplitude A_1 and the appearance of the higher harmonic contributions are due to the nonlinear nature of the Casimir effect. Since χ, α, and β, are all defined in terms of the derivatives of the potential energy evaluated at $\delta_{\min}$, in light of (8) one can relate Ω_0 and C through $\delta_{\min}$. Fig. 10 shows this three-way correspondence, where C and Ω_0 (normalized to the natural frequency $\omega(=\sqrt{k/m})$ of the harmonic oscillator in the absence of the Casimir effect) are plotted as functions of $\delta_{\min}$. In Fig. 11, we show several contours corresponding to equally spaced values $(0.05, 0.10, \ldots, 0.60)$ of the sum of the amplitudes, $A(= A_0 + A_1 + A_2 + A_3)$, as a function of A_1 and C (or $\delta_{\min}$). Also shown here is the curve that indicates the maximum allowed value of the sum A for a given value of $C < 0.075$ if oscillatory solutions in a separation state are to exist. This is the $A_{\max}$ curve, which is plotted thicker than the contours. For a given value of C (or $\delta_{\min}$), the maximum allowed value of A is determined by the three way intersection of the $A_{\max}$ curve, the dashed line corresponding to the C value of interest, and a single contour plot. For example, for $C = 0.04$, the $A_{\max}$ curve intersects the dashed line and

[8]The sign of the β term in the expression for A_3 is incorrect as given in [29].

the $A = 0.45$ contour at one and the same point; thus the maximum allowed value for A is 0.45 when $C = 0.04$. In Fig. 12(a)–(d), we have similar graphs displaying contours of the normalized amplitudes $A_0/A_1, -A_2/A_1$, and $-A_3/A_1$ as well as contours of the three-term approximation to the fundamental frequency, $\Omega(\cong \Omega_0 + \Omega_1 + \Omega_2)$, normalized to the natural frequency, ω. For reference, the $A_{\max}$ curve is also included in these figures. Fig. 12(b)–(d) shows normalized amplitudes that match the numerical results plotted in Fourier spectra, such as those in Fig. 9. Interestingly, the five-term, fourth-order Taylor series expansion of the potential energy function approximates the portion of the exact potential energy curve where oscillatory motion in separation states are allowed more accurately as C gets closer to $C_{\rm cr}$. Fig. 13 shows the exact and the approximate potential curves for $C = 0.04$.

Although our analysis here did not account for damping, the analysis has shown that the dynamics of an ACO device can change dramatically with C. Furthermore, we note that $C(=\Re/kw_0^5)$ itself is extremely sensitive to changes in w_0, which may be a controllable (e.g., piezoelectrically) physical dimension in a MEMS. For example, the depth of a sub-micrometer-deep micro-cavity can be electrically modulated if the cavity walls are made of piezoelectric materials. A thin silicon membrane suspended above a such a micro-cavity may be modeled as an ACO with variable C. The dependence of C on the fifth power of w_0 makes the ACO an attractive platform for rather sensitive sensors and detector system designs. Such designs will most likely have to take account of dissipative forces, especially if the dynamic characteristics of the ACO are to be exploited. For systems designed to work in the absence of vacuum, fluid (e.g., air) damping is the most important dissipative mechanism, followed by damping inherent to the oscillator. The fluid damping for an ACO will probably be of the squeeze-film type because of the extremely small separations required to exploit the Casimir effect [30]. In the absence of strong fluid damping, the contour plots in Figs. 11 and 12, along with the frequency variation curve in Fig. 10, may be used to study the Casimir effect in the periodic motion of a MEMS component wherein a linear restoring force is present and the oscillator's structural damping is negligible.

IV. The Casimir Switch

As shown in Section II, the ACO is a bi-stable system for $C < C_{\rm cr}$. Also, at the end of Section III A, we briefly discussed the possibility of changing C while keeping E constant (Fig. 4). The phase space plots for four of the potential energy curves in Fig. 4 are shown in Fig. 14 for $E = 0.046$. Any separation state, along with the contact state of an ACO device, may define an "open" and the "closed" states, respectively, of a Casimir switc.[9]

The switching of an ACO device between its open and closed states may be accomplished by changing the value of C and/or by introducing additional forces into the system. A large change in C, for example, can be affected by slightly varying the parameter w_0 as, for example, was discussed in the last paragraph of Section III. The additional forces may be electrostatic, mechanical, pneumatic, etc. We will briefly discuss some possibilities shortly. However, to quantify the stability of the open state of a switch, we shall first characterize the height of the potential energy barrier that separates the open state from the closed state for a given value of $C < C_{\rm cr}$. To this end, we define the quantity $P_{\rm bar}$ as a measure of the average pressure required to close the open switch by forcing the moveable plate to the right, past $\delta_{\max}$, and into the contact state

$$P_{\rm bar}(\delta_{\max}, \delta_{\min}) \equiv \frac{\Delta U}{\Delta w} = \frac{U(\delta_{\max}) - U(\delta_{\min})}{w_{\max} - w_{\min}} = \frac{1}{w_0}\frac{U(\delta_{\max}) - U(\delta_{\min})}{\delta_{\max} - \delta_{\min}} \tag{19}$$

where $w_{\max}$ and $\delta_{\max}$ are related to w_0 as in (3). Next, we substitute the expression in (5) for the potential energy $U(\delta)$ in (19), and use (8) to obtain a relation between $P_{\rm bar}, \delta_{\min}$, and $\delta_{\max}$ for a given value of $C < C_{\rm cr}$

$$P_{\rm bar} = \frac{E_k}{6w_0}[5(\delta_{\max} + \delta_{\min}) - 2]. \tag{20}$$

Defining the normalized barrier pressure $\Pi(\equiv P_{\rm bar}/kw_0)$ and noting that $\delta_{\min} + \delta_{\max}$ is always less than unity, we arrive at an upper limit of 0.5 for Π

$$\Pi = \frac{1}{6}[5(\delta_{\max} + \delta_{\min}) - 2] < \frac{1}{2}. \tag{21}$$

Using (8), we can find the variation of Π with C. This is shown in Fig. 15, wherein we see that the normalized pressure, Π, required to switch from the open state into the closed state decreases with increasing C.

The switching from an open to the closed state may be realized by increasing the parameter C from an initial value smaller than $C_{\rm cr}$ to one larger than $C_{\rm cr}$. In principle, this is possible even if the cavity between the parallel plates is air tight and contains a gas. In that case, $C_{\rm cr}$ is different than 0.0819. As discussed earlier, in an ACO device, the additional kinetic energy provided for the moveable plate by lowering the potential energy barrier would eventually be lost completely due to dissipative interactions, and the contact state would be established. Thus, to subsequently switch from the closed state back to an open state, reducing the value of C alone will most likely not be sufficient. This is true even though at or near contact, the expression for the Casimir pressure is no longer valid and the depth of the potential well is finite. The nature and the magnitudes of the attractive interactions at or near contact will be altered significantly by surface roughness and may no longer be represented by a simple expression of the type in (1). Nonetheless, experimental evidence suggests that in the contact state the attraction is rather strong [11]–[13]. The switch cannot be brought out of contact unless somehow $\delta_{\max}$, the value of which now depends on the form of the attractive forces near contact, is pushed to the right past $\delta = 1 - \xi$. One possibility to achieve this may be increasing w_0 by moving the left end of the spring in Fig. 3 further to the left and/or by increasing the spring constant, k, so that the elastic restoring

[9]Here, by an open state we shall mean a separation state for which $E = U_{\min}$.

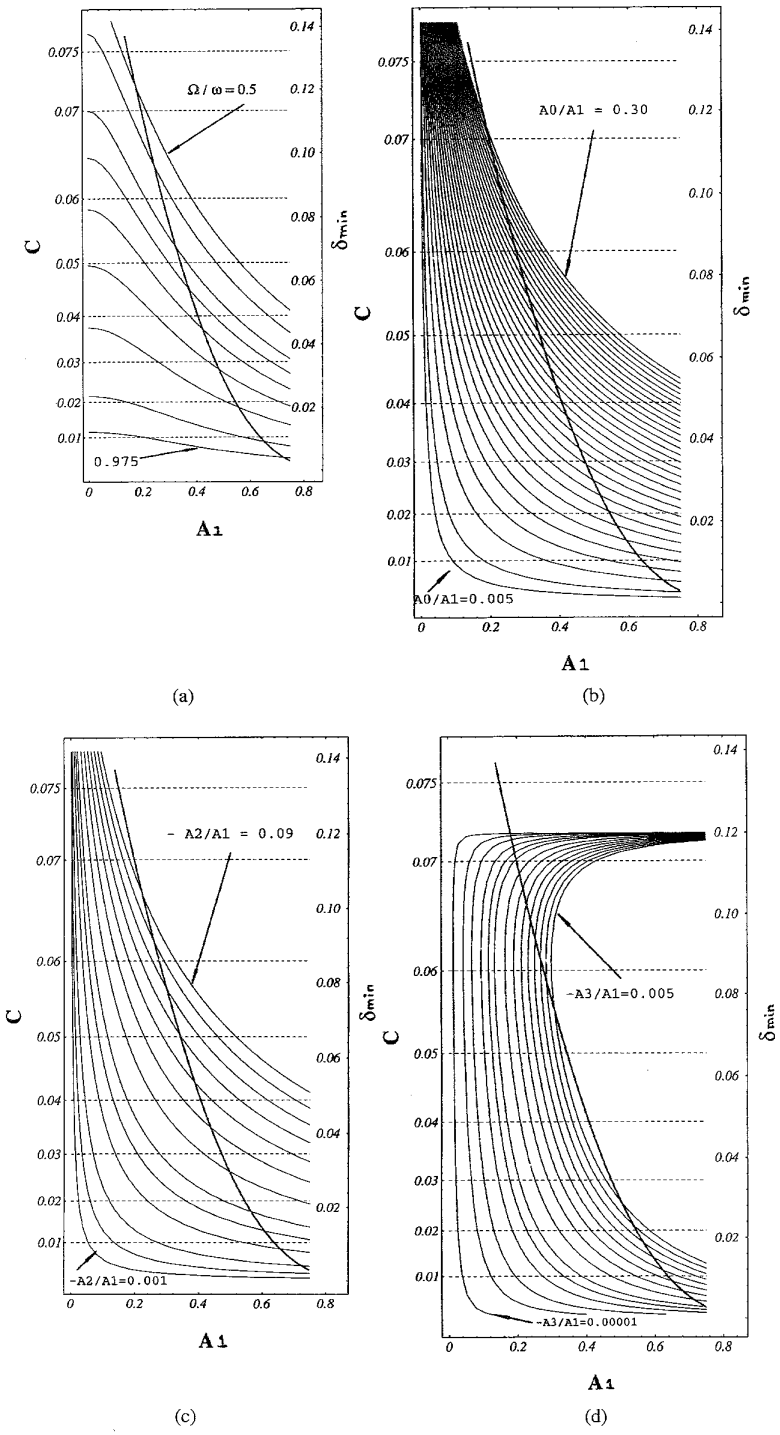

Fig. 12. While the $A_{\max}$ curve cannot be used here exactly as in Fig. 9, it helps in separating those values of A_1 that are definitely not allowed in separation state oscillations; this curve is included in all parts (a)–(d) of Fig. 10 and appears thicker than the contour plots. (a) Contour plots for the three-term approximation of the fundamental frequency, W, as normalized to the natural frequency, $\omega(=\sqrt{k/m})$, of the harmonic oscillator in the absence of the Casimir effect. The contours plotted correspond to normalized frequency values 0.5, 0.6, 0.7, 0.75, 0.8, 0.85, 0.9, 0.95, and 0.975. (b) Contour plots for the normalized zero frequency amplitude, A_0/A_1. Except for the first step, the successive contour values are equally separated: 0.005, 0.01, 0.02, 0.03, 0.04,...,0.28, 0.29, 0.30. (c) Contour plots for $-A_2/A_1$. Contour values are 0.0010, 0.0025, 0.0050, 0.0100, 0.0150, 0.0200, 0.0300, 0.0400, 0.0500, 0.0600, 0.0700, 0.0800, and 0.0900. (d) Contour plots for $-A_3/A_1$. Contour values are 0.00001, 0.00010, 0.00025, 0.00050, 0.00075, 0.00100, 0.00150, 0.00200, 0.00250, 0.00300, 0.00350, 0.00400, 0.00450, and 0.00500.

force on the moveable plate is increased until it is sufficient to overcome the attractive forces, thus releasing the moveable plate from contact. This may not always be practical. For example, a large enough increase in w_0 may induce plastic deformations in the "spring" before it serves to detach the parallel plates.

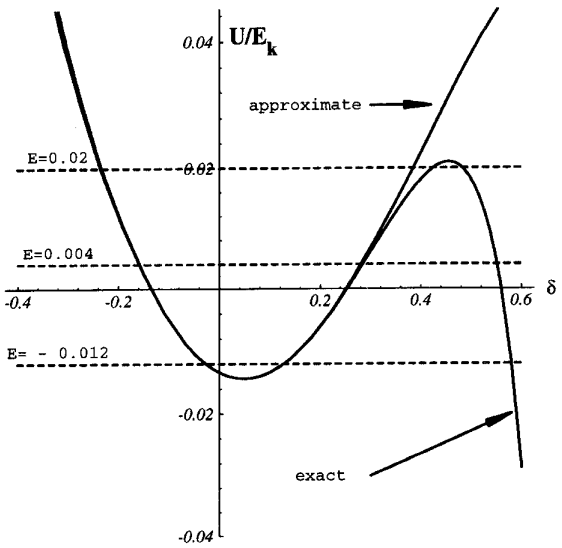

Fig. 13. Potential energy for $C = 0.04$. The two plots are those of the exact and the four-term Taylor series expansion about the local minimum for the potential function in (5).

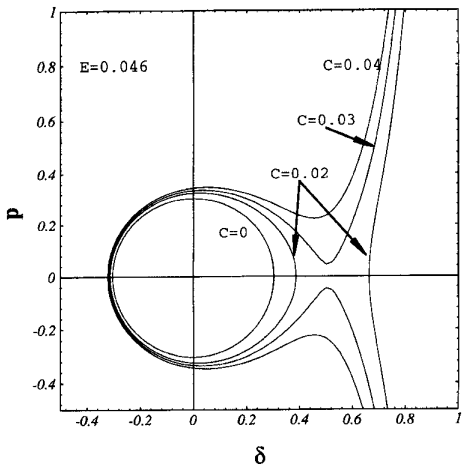

Fig. 14. The phase space plots corresponding to four of the C values in Fig. 4. The total normalized mechanical energy of the ACO in this figure is $E = 0.046$.

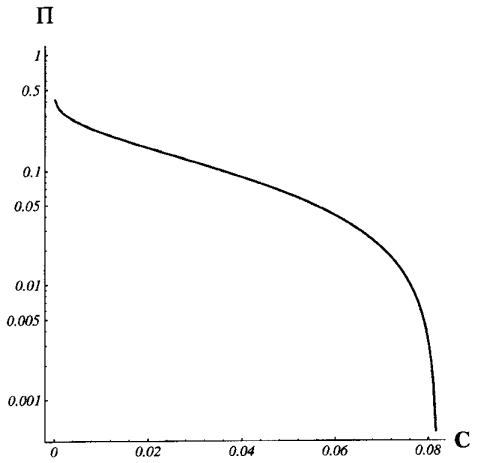

Fig. 15. The normalized pressure, Π, required to switch from the most stable open state, wherein the kinetic energy is zero($E = U_{\min}$), into the closed state has an upper bound of 0.5, and decreases with increasing C.

An alternative approach is to reduce the depth of the potential well corresponding to the contact state by introducing additional external forces. With a shallower potential well at contact, it may be possible to switch from the closed to an open state with smaller, more manageable changes in C, thus avoiding the extremely small values of this parameter. One such switch assist mechanism may be based on an air tight ACO with an isothermal gas trapped in between the parallel plates. This gas is assumed to obey the ideal gas law at constant temperature; thus its pressure is inversely proportional to its volume (i.e., inversely proportional to $1 - \delta$ for perfectly smooth surfaces on parallel plates). The modified potential energy per unit area with the trapped gas present is given as

$$U(\delta) = U_k + U_C + U_A = E_k\left(\frac{1}{2}\delta^2 - \frac{1}{3}\frac{C}{(1-\delta)^3} + C_A\left[\frac{-\delta}{1-\delta_{\min}} + \ln\left(\frac{1-\delta_{\min}}{1-\delta}\right)\right]\right) \tag{22a}$$

with the weight parameter C_A defined as

$$C_A \equiv \frac{P_i(1-\delta_{\min})}{k\,w_0}. \tag{22b}$$

Here, P_i is the gas pressure on both sides of the moveable plate in Fig. 3 when this plate is at $\delta_{\min}$, as defined by (7) applied to (5). Fig. 16 describes qualitatively what happens when C_A is changed in an ACO device. For a fixed value of C (i.e., for $C = 0.01$), as C_A is increased, the depth of the potential well at contact (i.e., at $\delta = 1 - \xi$) is reduced as $\delta_{\max}$ is shifted to the right. It is important to note that near the contact state (i.e., $\delta \cong 1 - \xi$), the curves in this figure are only qualitatively describing the system in that they show a negative slope for the potential there. The exact depth of the potential energy minimum at contact depends on the nature and the magnitude of the forces at contact. If the potential well at contact is sufficiently shallow, it may be possible to apply a small additional force, and/or to affect a small decrease in C, to switch from the closed to an open state.

We also note in Fig. 16 that the proposed pneumatic switch assist mechanism may serve to simply modify the height of the potential energy barrier and thus may also be utilized to control the relative stability of the open switch position. This may be used to design ACO threshold signal detectors, wherein the magnitude of the threshold signal is related to the height of the potential energy barrier.

If a dc voltage, V, is applied between the parallel plates. The resulting attractive force between the plates serves to reduce the height of the potential energy barrier between $\delta_{\min}$ and $\delta_{\max}$. This may be used in defining a lower bound on the strength of perturbations for which an initially open switch

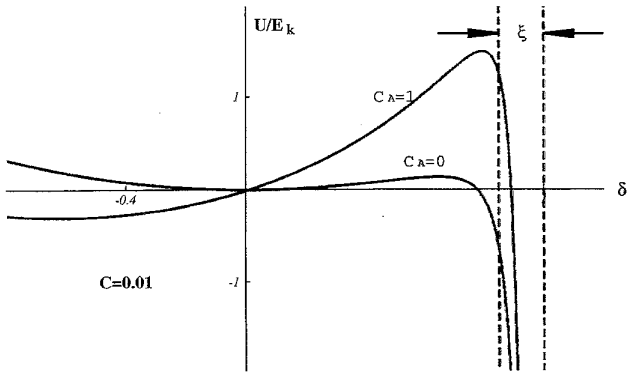

Fig. 16. For a fixed value of $C(= 0.01)$, the depth of the potential well at contact ($\delta = 1 - \xi$) is reduced as the initial gas pressure at $\delta = \delta_{\min}$ is increased on both sides of the moveable plate of an air tight ACO cavity. This can be used to lower the force required to switch from the closed to an open state. The increase in initial gas pressure, P_i , is reflected in an increase in C_A ($\propto P_i$).

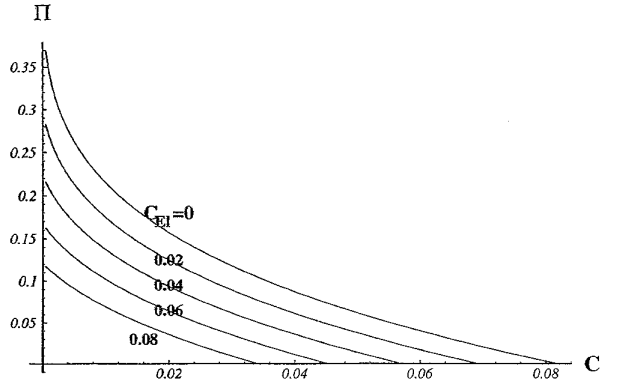

Fig. 17. For a given value of C, applying a dc voltage $V(C_{\rm El} \propto V^2)$ across the conducting parallel plates, separated from each other at contact by an insulating layer, will reduce the stability of the open switch position against perturbations.

will close. The corresponding additional potential energy term, $U_{\rm El}$, is given below

$$U(\delta) = U_k + U_C + U_{\rm El} = E_k\left(\frac{1}{2}\delta^2 - \frac{1}{3}\frac{C}{(1-\delta)^3} - C_{\rm El}\frac{1}{1-\delta}\right) \quad (23a)$$

where the weight factor $C_{\rm El}$ is defined as

$$C_{\rm El} \equiv \frac{\varepsilon_0 V^2}{2E_k\, w_0} \quad (23b)$$

with ε_0 denoting the effective dielectric permittivity of the medium between the conducting surfaces. This medium consists of a thin insulating layer (on one or both conducting surfaces) that isolates the conductors when the switch is closed (e.g., an oxide layer on heavily doped SCS or polysilicon) and a gas that fills the space between the plates when the switch is open. Equation (23) assumes that the gas is *not* trapped in this space. The variation of the normalized barrier pressure with C is plotted for several values of $C_{\rm El}$ in Fig. 17. This figure also shows the value of $C_{\rm cr}$ (corresponding to zero barrier pressure) reducing with increased applied voltage.

In closing this section, we note that at least one of the two switch positions in a functional Casimir switch may be maintained with no electric power required.

V. Summary and Conclusion

The Anharmonic Casimir Oscillator (ACO), a simple dynamic system that includes the attractive parallel plate Casimir pressure, has been modeled. We have characterized this system by the positive dimensionless constant $C(\equiv \Re/kw_0^5)$. For $C > C_{\rm cr}(\cong 0.082)$, an ACO device is always in its "contact state," in which state the parallel plates are in contact with each other. For $C < C_{\rm cr}$, the ACO may be a bi-stable system. The moveable plate can execute anharmonic oscillations about one of its stable equilibrium states; this is an ACO device in a "separation" state. The other stable equilibrium state is the contact state. Oscillations of the ACO in the separation state were investigated analytically and computationally. It was argued that the sensitivity of the system dynamics to changes in C and the feasibility of changing C in a MEMS device made the ACO a platform for designing sensitive detectors and sensors.

Next, we considered a mechanical switch based on the ACO. External forces, or changes in the system parameters (changing C) can cause an ACO device to switch from an open state to the closed state. It was shown that the open position of such a switch has limited stability against perturbations and that this stability may be improved by introducing switch assist mechanisms. We have also argued that the switching action from open to closed may be realized by merely changing C, while switching from the closed to an open position will most likely need to be effected in the presence of switch assist mechanisms.

The ACO modeling presented here was intended to provide some insight into the role of the Casimir force in more complex MEMS. It was also intended to draw attention to the roles that quantum fluctuational forces in general may be playing in MEMS as device dimensions and separations become smaller. With a good understanding of the elastic forces involved, the ACO model may be used as a basis to estimate the contribution of the Casimir effect to the stiction of device components in MEMS. Furthermore, it appears that the attractive force between parallel surfaces may not always have to be dealt with as a nuisance; rather, it may be manipulated to perform useful tasks just as capillary forces have been utilized to actuate MEMS components. Dynamic characteristics of the ACO may be used to design small gap resonators based on the Casimir effect.

Acknowledgment

The authors would like to thank R. L. Forward for sharing his knowledge and ideas on the subject of the Casimir effect. Also, they would like to thank H. Busta for reviewing the manuscript and for offering insightful questions and comments. F. M. Serry is grateful for the friendship and the opportunity to work with G. J. Maclay and D. Walliser.

REFERENCES

[1] T. Hirano, T. Furuhata, K. J. Gabriel, and H. Fujita, "Design, fabrication, and operation of submicron gap comb-drive microactuators," *J. Microelectromechanical Syst.*, vol. 1, no. 1, pp. 52–59, Mar. 1992.

[2] W. Chen and H. Ahmed, "Fabrication of high aspect ratio silicon pillars of <10 nm diameter," *Appl Phys. Lett.*, vol. 63, no. 8, pp. 1116–1118, Aug. 23, 1993.

[3] H. B. G. Casimir, "On the attraction between two perfectly conducting plates," in *Proc. Koninkl. Ned. Akad. Wetenschap.*, 1948, vol. 51, pp. 793–795.

[4] L. S. Brown and G. J. Maclay, "Vacuum stress between conducting plates: An image solution," *Phys. Rev.*, vol. 184, pp. 1272–1279, 1969.

[5] J. Schwinger, L. L. DeRaad Jr., and K. A. Milton, "Casimir effect in dielectrics," *Ann. Phys.*, vol. 115, pp. 1–23, 1978.

[6] K. A. Milton, L. L. DeRaad Jr., and J. Schwinger, "Casimir self-stress on a perfectly conducting spherical shell," *Ann. Phys.*, vol. 115, pp. 388–403, 1978.

[7] T. H. Boyer, "Quantum electromagnetic zero-point energy of a conducting spherical shell and the Casimir model for a charged particle," *Phys. Rev.*, vol. 174, no. 5, pp. 1764–1776, Oct. 1968.

[8] E. M. Lifshitz, "The theory of molecular attractive forces between solids," *Sov. Phys. JETP*, vol. 2, pp. 73–83, 1956.

[9] B. V. Derjagin, N. V. Churaev, and V. M. Muller, *Surface Forces*. New York: Consultants Bureau, 1987, ch. 4.

[10] E. Elizalde and A. Romeo, "Essentials of the casimir effect and its computation," *Am. J. Phys.*, vol. 59, no. 8, pp. 711–719, Aug. 1991.

[11] C. Linder and N. F. De Rooij, "Investigations on free-standing polysilicon beams in view of their applications as transducers," *Sensors and Actuators A (Physical)*, vol. 21–23, pp. 1053–1059, Apr. 1990.

[12] P. R. Scheeper, J. A. Voorthuyzen, W. Olthuis, and P. Bergveld, "Investigation of attractive forces between PECVD silicon nitride microstructures and an oxidized silicon substrate," *Sensors and Actuators A*, vol. 30, pp. 231–239, 1992.

[13] C. H. Mastrangelo and H. Hsu, "Mechanical stability and adhesion of microstructures under capillary forces, part I and II," *J. Microelectromechanical Syst.*, vol. 2, no. 1, pp. 33–55, Mar. 1993.

[14] M. Bordag, G. L. Klimchitskaya, and V. M. Mostepanenko, "Corrections to the Casimir force between plates with stochastic surfaces," *Phys. Lett. A*, vol. 200, pp. 95–102, Apr. 17, 1995.

[15] ——, "Casimir force between two parallel plates with small distortions of different types," *Modern Phys. Lett. A*, vol. 9, no. 27, pp. 2515–2526, 1994.

[16] S. K. Karepanov, M. Yu. Novikov, and A. S. Sorin, "The influence of one-dimensional flat boundary distortions on the Casimir force," *Nuovo Cimento*, vol. 100 B, no. 3, pp. 411–415, Sept. 1987.

[17] B. V. Derjaguin, Y. I. Rabinovich, and N. V. Churaev, "Direct measurement of molecular forces," *Nature*, vol. 272, pp. 313–318, 23 Mar., 1978.

[18] W. Arnold, S. Hunklinger, and K. Dransfeld, "Influence of optical absorption on the van der Waals interaction between solids," *Phys. Rev. B*, vol. 19, no. 12, pp. 6049–6056, June 15, 1979.

[19] P. H. G. M. van Blokland and J. T. G. Overbeek, "van der Waals forces between objects covered with a chromium layer," *J. Chem. Soc.—Faraday Transactions I*, vol. 74, pp. 2637–2651, 1978.

[20] H. B. G. Casimir and D. Podler, "The influence of retardation on the London—van der Waals forces," *Phys. Rev.*, vol. 73, no. 4, pp. 360–372, 1948.

[21] G. Plunien, B. Muller, and W. Greiner, "The Casimir effect," *Physics Reports (Review Section of Phys. Lett.)*, vol. 134, nos. 2, 3, pp. 87–193, 1986.

[22] I. J. R. Aitchison, "Nothing's plenty: The vacuum in modern quantum field theory," *J. Contemp. Phys.*, vol. 26, no. 4, pp. 333–391, 1985.

[23] J. Ambjorn and S. Wolfram, "Properties of the vacuum. 1. Mechanical and thermodynamic. 2. Electrodynamic," *Ann. Phys.*, vol. 147, pp. 1–56, 1983.

[24] B. V. Deryagin, I. I. Abrikosova, and E. M. Lifshitz, "Molecular attraction in the condensed state," *Advances in Physical Sciences (USSR)*, vol. 64, no. 3, pp. 493–528, 1958.

[25] R. Matthews, "Inertia: Does empty space put up the resistance?" *Science*, vol. 263, pp. 612–613, Feb. 4, 1994.

[26] Y. Srivastava, A. Widom, and M. H. Friedman, "Microchips as precision quantum electrodynamic probes," *Phys. Rev. Lett.*, vol. 55, no. 21, Nov. 18, 1985.

[27] B. G. Levi, "New evidence confirms old predictions of retarded forces," *Physics Today*, vol. 47, no. 4, pp. 18–20, Apr. 1993.

[28] "Mathematica, A system for doing mathematics by computer, version 2.2," Wolfram Research Inc., Champaign, IL, 1994.

[29] L. D. Landau and E. M. Lifshitz, *Mechanics*. Oxford: Pergamon, 1960, ch. 28.

[30] F. M. Serry, P. Neuzil, R. Vilasuso, and G. J. Maclay, "Air-damping of resonant AFM micro-cantilevers in the presence of a nearby surface," in *Proc. Microstructures and Microfabricated Systems II,* June 1995, Electrochemical Society, vol. 95-27, pp. 83–89.

F. Michael Serry received the B.S. degree in physics from Elmhurst College, Elmhurst, IL, in 1987, and the M.S. degree in physics from the University of New Mexico, Albuquerque, NM, in 1990. He received the M.S. degree in electrical engineering and computer science from the University of Illinois at Chicago (UIC) in 1995 and is currently a Ph.D. candidate at UIC.

Dirk Walliser received the M.S. degree in physics from the University of New Mexico, Albuquerque, NM, in 1988, and the Ph.D. degree in theoretical physics from the University of Hannover and DESY, Hamburg, Germany, in 1992.

Since then he has held Postdoctoral Research Fellowships at DESY (1992) and at the Fermi National Accelerator Laboratory at Batavia, IL (1993). He is currently employed as a Research Associate at the Daimler Benz company in Germany.

G. Jordan Maclay (M'83) received the Ph.D. degree in physics from Yale University in 1972.

Since 1980 he has been a Professor of Electrical Engineering in the Department of Electrical Engineering and Computer Science at the University of Illinois at Chicago (UIC). He has worked extensively with sensor technology, particularly with microsensors and microsensor systems. He is Director of the Microfabrication Applications Laboratory at UIC. He has seven patents and over 50 publications in microsensors and microelectronics.

In 1991, Dr. Maclay received the Science and Technology Advocate of the Year Award from the American Electronics Association.